Research in Astronomy and Astrophysics, 24:015022 (12pp), 2024 January https://doi.org/10.1088/1674-4527/ad1367

Periodic Variation Studies of the Two Short Period W UMa-type Eclipsing Binaries: LX Lyn and V0853 Aur

Xu Zhang[1] and Bin Zhang[1,2,3]
[1] School of Physics and Electronic Science, Guizhou Normal University, Guiyang 550001, China; zhangb1256@163.com
[2] Guizhou Provincial Key Laboratory of Radio Astronomy and Data Processing, Guizhou Normal University, Guiyang 550025, China
Received 2023 October 23; revised 2023 November 21; accepted 2023 December 4; published 2024 January 15

Abstract

In this paper, new light curves (LCs) of contact eclipsing binary (CEB) systems LX Lyn and V0853 Aur are presented and analyzed by using the 2015 version of the Wilson–Devinney (W-D) code. In order to explain their asymmetric LCs, cool starspots on the components were employed. It is suggested that their fill-out degrees are $f = 12.0\%$ (LX Lyn) and $f = 26.3\%$ (V0853 Aur). At the same time, we found that LX Lyn is a W-type eclipsing binary (EB) with an orbital inclination of $i = 84^{\circ}.88$ and a mass ratio of $q = 2.31$. V0853 Aur is also a W-type CEB with a mass ratio of $q = 2.77$ and an orbital inclination of $i = 79^{\circ}.26$. Based on all available times of light minimum, their orbital period changes are studied by using the $O - C$ method. The $O - C$ diagram of LX Lyn reveals a cyclic oscillation with a period of about 14.84 yr and an amplitude of 0.0019 days, which can be explained by the light-travel time effect (LTTE) due to the presence of a third body with a minimum mass of $0.06M_{\odot}$. For V0853 Aur, it is discovered that the $O - C$ diagram of the system also shows a cyclic oscillation with a period of 9.64 yr and an amplitude of 0.03365 days. The cyclic oscillation of V0853 Aur can be attributed to the LTTE by means of a third body with a mass no less than $3.77M_{\odot}$. The third body may play an important role in the formation and evolution of these systems.

Key words: stars: activity – (stars:) binaries (including multiple): close – (stars:) binaries: eclipsing – (stars:) brown dwarfs – stars: evolution – stars: formation

1. Introduction

The formation and evolution of short-period W UMa-type eclipsing binaries (EBs) are still an open question. It is predicted that they were formed from initially short-period cold-separated binaries, experiencing angular momentum loss (AML) (e.g., Vant Veer 1979; Qian 2003; Qian 2017; Li et al. 2007; Qian et al. 2018) controlled by magnetic activity and evolved into contact configurations with very low mass ratio (e.g., Li et al. 2004). Because these binaries have a common convective envelope (CCE) (Lucy 1968), the surface effective temperature of the components is very close, and the depth of two occultations in the light curves (LCs) is almost equal. Binnendijk (1970) made a more accurate comparison of the temperatures and divided them into A and W types. More importantly, the two components of a contact eclipsing binary (CEB) can exchange matter through the Lagrangian point, which can change the evolutionary track of each star in the system. Moveover, it is found that many of the CEB systems have an extra companion (Pribulla & Rucinski 2006), such as J0344 (Zhang et al. 2020), WW Dra (Liao & Qian 2010), V752 Cen (Zhou et al. 2019), PZ UMa (Zhou & Soonthornthum 2019), J1155 (Zhang et al. 2019) and NSVS 01286630 (Zhang et al. 2018b). The existence of the third body can make the $O - C$ values of the binary system changed periodically, which is also called the light-travel time effect (LTTE).

The W UMa-type binaries have an obvious periodic cutoff phenomenon at ~0.22 days (Rucinski 1992). According to the latest observations, some CEBs with a period shorter than 0.22 days have been discovered. For example, Davenport et al. (2013) reported a CEB SDSS J001641-000925 with a period of 0.19856 days, and Nefs et al. (2012) also discovered nine EB candidates with periods less than 0.22 days from the Wide Field Camera Transit Survey. Meanwhile, Drake et al. (2014) identified 231 binaries with orbital periods less than 0.22 days by using data from the Catalina Sky Survey. After that, Zhang & Qian (2020) proposed a new period cutoff limit at 0.15 days based on many observations and theoretical analysis. The detailed reasons for the period cutoff phenomenon are still not clear now. There are several explanations for that: Rucinski (1992) first proposed the complete convection limit to explain this phenomenon, but it is limited by the contact structure model. Then, some researchers thought that because the timescale of AML is very long, it is difficult to form this kind of binary system (Stępień 2006; Stępień & Gazeas 2012). In addition, Jiang et al. (2012) believe that it is the result of mass transfer instability during the initial detached binaries.

[3] Author to whom any correspondence should be addressed.

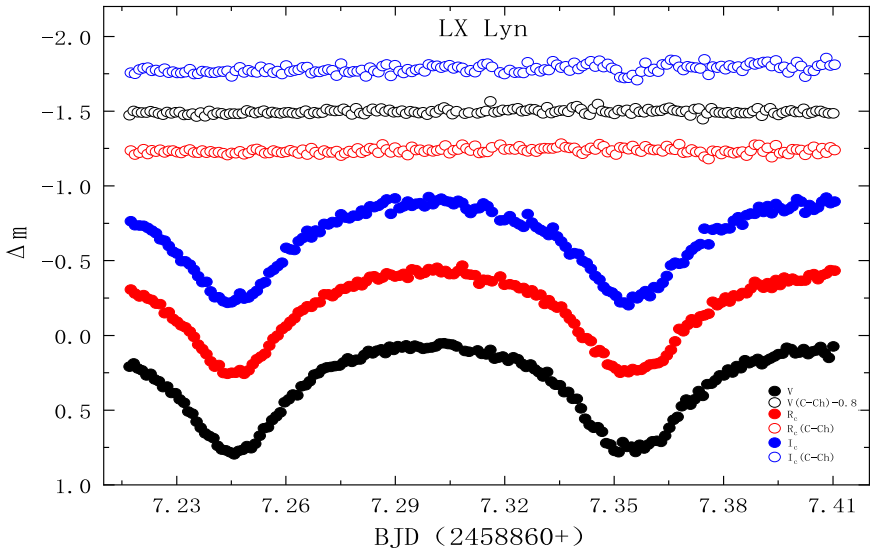

Figure 1. The observational LCs of LX Lyn in VR_cI_c bands.

Thanks to the Wide Angle Search for Planets (SuperWASP) survey, LX Lyn (= 1SWASP J080150.03+471433.8) was first discovered and identified as a W UMa-type binary candidate with an orbital period of 0.2175 days (Norton et al. 2011). Then, the first photometric solutions were carried out by Terrell & Gross (2014). Subsequently, Dimitrov et al. (2015) performed a low-resolution spectroscopic analysis and found that it is an over-contact EB. After that, Darwish et al. (2017) explored the relationships between mass–luminosity and mass–radius of the two components, and they ascertained that the less massive component is above the empirical M–R relation position (Lucy 1973; Eker et al. 2015). It is found that LX Lyn is an important case to study the formation of a CEB with an orbital period near 0.22 days (Loukaidou et al. 2022).

V0853 Aur (= NSVS 4484038 = 1SWASP J055416.98 +442534.0) was first discovered by the Northern Sky Variability Survey (Hoffman et al. 2009). Subsequently, the SuperWASP project determined its orbital period as 0.218495 days (Lohr et al. 2013). Then, its first photometric solutions in the B and V-band were obtained, and it was found that the target is a CEB system (Zhang et al. (2014b)). Dimitrov et al. (2015) acquired its low resolution spectrum and mass ratio of $q = 0.792$. Thereafter, using the $O-C$ method, Lu et al. (2020) first studied its orbital period variations. They reported a cyclic oscillation, which may be caused by the magnetic activity or a third body.

2. Photometric Observation

We obtained new multi-band LCs of LX Lyn and V0853 Aur by using the 60 cm reflecting telescope at the Xinglong Station of National Astronomical Observatories, Chinese Academy of Sciences. The LCs of LX Lyn in VR_cI_c bands were acquired in 2020 (January 18), and are displayed in Figure 1. Two stars near the target are selected as the comparison star and check star (see Table 1). We also adopted the Simple Aperture Photometry (SAP) LCs of LX Lyn. The Transiting Exoplanet Survey Satellite (TESS) LCs of LX Lyn are from sector 20 with 30 minute cadence and sector 47 with 10 minute cadence. Based on our observations, we obtained 10 light minima times and listed them in Table 2.

Table 1
Coordinates of the Variable, Comparison and Check Stars

Targets	Name	α_{2000}	δ_{2000}
Variable star	LX Lyn	$08^h01^m50\overset{s}{.}030$	$+47^h14^m33.43$
Comparison	GSC 3408-01475	$08^h01^m36\overset{s}{.}295$	$+47^h10^m18\overset{s}{.}88$
Check	GSC 3408-00253	$08^h02^m0\overset{s}{.}415$	$+47^h14^m5\overset{s}{.}14$
Variable star	V0853 Aur	$05^h54^m17\overset{s}{.}014$	$+44^h25^m34\overset{s}{.}00$
Comparison	GSC 2924-1387	$05^h54^m18\overset{s}{.}274$	$+44^h27^m43\overset{s}{.}45$
Check	GSC 2924-1089	$05^h54^m14\overset{s}{.}436$	$+44^h30^m18\overset{s}{.}61$

For V0853 Aur, we also obtained new photometric LCs in the VR_cI_c bands on 2021 November 30 and 2020 December 25. The observed images were reduced by using the software IRAF, and the corresponding LCs are shown in Figure 2. At the same time, we collected the TESS LCs from sector 19 with 30 minute cadence. In addition, 13 new light minima times were determined and are listed in Table 3.

3. The Analysis of Orbital Period Changes

The $O-C$ method is a useful way to study orbital period changes of binary systems (Qian et al. 2013; Zhang et al. 2018b). For CEB, the orbital period modulations are very common, such as parabolic, cyclic, or both. Exploring the

Table 2
($O - C$) Data for LX Lyn

BJD	Error (day)	Epoch	($O - C$) (day)	Reference	BJD	Error (day)	Epoch	($O - C$) (day)	Reference
2454410.07682	0.00049	0	0.00000	(1)	2456714.29857	0.00010	10593.5	−0.00222	(4)
2454410.18558	0.00066	0.5	0.00000	(1)	2456714.29867	0.00010	10593.5	−0.00212	(4)
2454422.80028	0.00058	58.5	−0.00105	(1)	2456714.40677	0.00020	10594	−0.00278	(4)
2454423.12372	0.00340	60	−0.00388	(1)	2456714.40707	0.00030	10594	−0.00248	(4)
2454427.47905	0.00068	80	0.00119	(1)	2456714.40717	0.00050	10594	−0.00238	(4)
2454427.58644	0.00073	80.5	−0.00018	(1)	2457036.76528	0.00049	12076	0.00147	(5)
2454427.69585	0.00044	81	0.00048	(1)	2457036.87475	0.00144	12076.5	0.00219	(5)
2454427.80304	0.00037	81.5	−0.00109	(1)	2457227.52315	0.00027	12953	0.00044	(5)
2454437.80854	0.00051	127.5	−0.00119	(1)	2457395.87622	0.00041	13727	−0.00155	(5)
2454437.91958	0.00071	128	0.00110	(1)	2457395.98327	0.00044	13727.5	−0.00326	(5)
2454438.02643	0.00051	128.5	−0.00081	(1)	2457395.98335	0.00046	13727.5	−0.00318	(5)
2454438.13735	0.00044	129	0.00135	(1)	2457396.09363	0.00042	13728	−0.00165	(5)
2454497.29966	0.00053	401	0.00013	(1)	2457396.09367	0.00039	13728	−0.00161	(5)
2454497.40854	0.00030	401.5	0.00025	(1)	2457747.05076	0.00094	15341.5	−0.00175	(5)
2454497.51821	0.00031	402	0.00116	(1)	2457747.05097	0.00090	15341.5	−0.00154	(5)
2454502.84573	0.00047	426.5	−0.00038	(1)	2457747.15951	0.00079	15342	−0.00176	(5)
2454502.95521	0.00030	427	0.00034	(1)	2457747.15985	0.00050	15342	−0.00142	(5)
2454503.06385	0.00024	427.5	0.00022	(1)	2458843.64628	0.00032	20383	0.00198	(6)
2454532.75422	0.00034	564	0.00007	(1)	2458843.75493	0.00035	20383.5	0.00187	(6)
2454532.86353	0.00040	564.5	0.00062	(1)	2458843.86392	0.00022	20384	0.00211	(6)
2454532.97297	0.00066	565	0.00130	(1)	2458847.34425	0.00010	20400	0.00223	(6)
2454533.07892	0.00050	565.5	−0.00150	(1)	2458847.45302	0.00005	20400.5	0.00224	(6)
2454536.23483	0.00038	580	0.00047	(1)	2458847.56182	0.00010	20401	0.00229	(6)
2454536.34427	0.00057	580.5	0.00115	(1)	2458852.34718	0.00014	20423	0.00236	(6)
2454544.28408	0.00054	617	0.00174	(1)	2458852.45564	0.00013	20423.5	0.00206	(6)
2454544.39179	0.00054	617.5	0.00069	(1)	2458852.56472	0.00008	20424	0.00239	(6)
2454544.50144	0.00139	618	0.00159	(1)	2458858.21996	0.00056	20450	0.00229	(6)
2454545.91315	0.00091	624.5	−0.00054	(1)	2458858.32859	0.00009	20450.5	0.00216	(6)
2454554.39578	0.00096	663.5	−0.00092	(1)	2458858.43748	0.00014	20451	0.00230	(6)
2455563.54706	0.00020	5303	−0.00120	(2)	2458862.35283	0.00012	20469	0.00241	(6)
2455563.54836	0.00020	5303	0.00010	(2)	2458862.46119	0.00012	20469.5	0.00202	(6)
2455563.65711	0.00020	5303.5	0.00010	(2)	2458862.57031	0.00008	20470	0.00238	(6)
2455563.65745	0.00020	5303.5	0.00043	(2)	2458866.59414	0.00017	20488.5	0.00222	(6)
2455568.44242	0.00020	5325.5	0.00012	(2)	2458866.70324	0.00016	20489	0.00256	(6)
2455568.44243	0.00020	5325.5	0.00013	(2)	2458866.81161	0.00011	20489.5	0.00218	(6)
2455568.55117	0.00020	5326	0.00011	(2)	2458867.24566	0.00013	20491.5	0.00120	(7)
2455568.55120	0.00020	5326	0.00015	(2)	2458867.24585	0.00011	20491.5	0.00139	(7)
2456625.98906	0.00022	10187.5	−0.00145	(5)	2458867.24593	0.00015	20491.5	0.00147	(7)
2456626.09820	0.00023	10188	−0.00106	(5)	2458867.35496	0.00019	20492	0.00174	(7)
2456702.66106	0.00050	10540	−0.00278	(3)	2458867.35543	0.00023	20492	0.00221	(7)
2456702.77357	0.00040	10540.5	0.00097	(3)	2458867.35596	0.00034	20492	0.00274	(7)
2456702.88267	0.00020	10541	0.00131	(3)	2458867.46267	0.00014	20492.5	0.00070	(7)
2456703.64377	0.00010	10544.5	0.00112	(3)	2458867.46329	0.00018	20492.5	0.00132	(7)
2456703.75247	0.00020	10545	0.00106	(3)	2458867.46524	0.00015	20492.5	0.00327	(7)
2456703.86187	0.00110	10545.5	0.00170	(3)	2459575.36102	0.00035	23747	0.00299	(7)
2456714.29807	0.00020	10593.5	−0.00272	(4)					

Reference: (1) SuperWASP, (2) Dimitrov et al. (2015), (3) Terrell & Gross (2014), (4) Darwish et al. (2017), (5) ASAS-SN, (6) TESS, (7) This paper.

causes of these modulations is very important for a detailed study of the dynamical evolution of binary systems and search for a third body. Generally, mass loss through stellar winds and mass transfer between the components can be caused by secular period variations. In addition, cyclic changes of the orbital period can be explained by the Applegate mechanism or the LTTE (Irwin 1952; Applegate 1992; Borkovits et al. 2016).

3.1. LX Lyn

A total of 91 light minima times are used to analyze the orbital period changes of LX Lyn. Among them, six are from Terrill et al. (2014), eight are from Dimitrov et al. (2015) and six are from Darwish et al. (2017). In addition, the TESS space mission, SuperWASP, and All-Sky Automated Survey for SuperNovae (ASAS-SN) provided another 61 eclipse times.

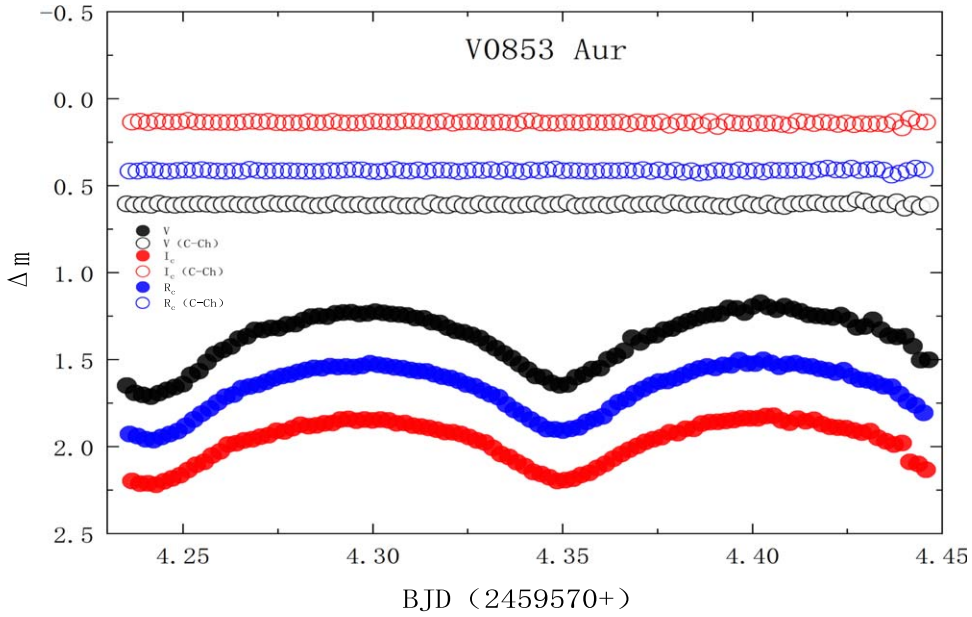

Figure 2. The observational LCs of V0853 Aur in VR_cI_c bands.

The $O-C$ values were calculated with the following linear ephemeris,

$$\begin{aligned}\text{Min.I(BJD)} &= 2454410.07682(\pm 0.00049)\\ &\quad + 0^d.217513 \times E. \end{aligned} \tag{1}$$

The calculated $O-C$ values of LX Lyn are listed in Table 2.

After fitting, we corrected the ephemeris to the following equation,

$$\begin{aligned}\text{Min. I(BJD)} &= 2454410.07500(\pm 0.00009)\\ &\quad + 0.^d217513184(\pm 0.000000008) \times E\\ &\quad + 0.00191(\pm 0.000071)\\ &\quad \times \sin(0^\circ.01446 \times E + 64^\circ.8642(\pm 2^\circ.909)).\end{aligned} \tag{2}$$

It should be noted that a circular orbit was assumed during our analysis. Moreover, weights of $1/\sigma^2$ were assigned to these data, where σ is the error. The corresponding $O-C$ curve is depicted in Figure 3.

3.2. V0853 Aur

We collected 61 light minima times of V0853 Aur from published literature in the present work (Christian et al. 2006; Zhang et al. 2014b; Dimitrov & Kjurkchieva 2015; Hong-Peng Lu et al. 2020). At the same time, based on several sky surveys, we also obtained some light minima times, such as SuperWASP (23), ASAS-SN (5), and TESS (8). During our calculation, the following linear ephemeris is adopted,

$$\begin{aligned}\text{Min.I(BJD)} &= 2454387.677781(\pm 0.003)\\ &\quad + 0^d.21855 \times E. \end{aligned} \tag{3}$$

All the $O-C$ values we used are listed in Table 3. Applying the least squares method, the new formula is obtained as follows,

$$\begin{aligned}\text{Min.I(BJD)} &= 2454387.69248(\pm 0.00006)\\ &\quad + 0.^d218548472(\pm 0.000000005) \times E\\ &\quad + 0.0336507(\pm 0.000058)\\ &\quad \times \sin(0^\circ.02235 \times E - 40^\circ.1788(\pm 0^\circ.098)).\end{aligned} \tag{4}$$

The final $O-C$ diagram is plotted in Figure 4. It is apparent that the $O-C$ diagram of V0853 Aur exhibits a periodic oscillation.

4. Photometric Solutions Obtained with the Wilson–Devinney Method

In order to study the targets well, it is necessary to obtain the photometric solutions of these two systems. During our analysis, the 2015 version of the Wilson–Devinney (W-D) program was used (Wilson & Devinney 1971; Wilson 1979, 1990, 1993; Van Hamme & Wilson 2003, 2007; Wilson 2008; Wilson et al. 2010; Wilson 2012, and Wilson & Van Hamme 2014). The adjustable parameters are: the orbital inclination, i; effective temperature of the secondary component, T_2; luminosity contributions of the primary component, L_1; the dimensionless potentials, Ω_1 and Ω_2; and the mass ratio, q. Moreover, two parameters in our fit are fixed, the bolometric

Table 3
$O - C$ Data for V0853 Aur

BJD	Error (day)	Epoch	$(O - C)$ (day)	Reference	BJD	Error(day)	Epoch	$(O - C)$ (day)	Reference
2454387.67778	0.00300	0	0.00000	(1)	2456671.07877	0.00500	10448	−0.00941	(4)
2454388.66081	0.00047	4.5	−0.00045	(2)	2456671.18897	0.00500	10448.5	−0.00849	(4)
2454388.77052	0.00052	5	−0.00001	(2)	2456671.18917	0.00500	10448.5	−0.00829	(4)
2454389.64378	0.00100	9	−0.00095	(1)	2456671.29687	0.00500	10449	−0.00986	(4)
2454392.70278	0.00200	23	−0.00165	(1)	2456671.29747	0.00500	10449	−0.00926	(4)
2454393.57633	0.00062	27	−0.00230	(2)	2456672.06287	0.00500	10452.5	−0.00879	(4)
2454393.57703	0.00034	27	−0.00160	(2)	2456672.06297	0.00500	10452.5	−0.00869	(4)
2454393.68478	0.00200	27.5	−0.00312	(1)	2456673.04527	0.00500	10457	−0.00986	(4)
2454393.68567	0.00068	27.5	−0.00224	(2)	2456673.04697	0.00500	10457	−0.00817	(4)
2454393.68568	0.00033	27.5	−0.00223	(2)	2456673.15547	0.00500	10457.5	−0.00894	(4)
2454393.79404	0.00061	28	−0.00314	(2)	2456673.15557	0.00500	10457.5	−0.00884	(4)
2454393.79486	0.00058	28	−0.00232	(2)	2456673.26377	0.00500	10458	−0.00991	(4)
2454393.90527	0.00047	28.5	−0.00119	(2)	2456673.26397	0.00500	10458	−0.00971	(4)
2454394.66878	0.00300	32	−0.00260	(1)	2456674.03037	0.00500	10461.5	−0.00824	(4)
2454397.61851	0.00046	45.5	−0.00330	(2)	2456674.03047	0.00500	10461.5	−0.00814	(4)
2454397.61878	0.00500	45.5	−0.00302	(1)	2456674.13817	0.00500	10462	−0.00971	(4)
2454397.72615	0.00095	46	−0.00493	(2)	2456674.13827	0.00500	10462	−0.00961	(4)
2454397.84294	0.00078	46.5	0.00258	(2)	2456674.24777	0.00500	10462.5	−0.00939	(4)
2454398.60278	0.00500	50	−0.00250	(1)	2456674.24857	0.00500	10462.5	−0.00859	(4)
2454405.59178	0.00300	82	−0.00710	(1)	2456681.78358	0.00031	10497	−0.01355	(5)
2454405.70278	0.00200	82.5	−0.00537	(1)	2456681.89311	0.00029	10497.5	−0.01330	(5)
2454406.57678	0.00200	86.5	−0.00557	(1)	2457683.92001	0.00030	15082.5	−0.03815	(6)
2454406.68678	0.00300	87	−0.00485	(1)	2457697.90381	0.00030	15146.5	−0.04155	(6)
2454407.56056	0.00046	91	−0.00527	(2)	2457698.01251	0.00050	15147	−0.04212	(6)
2454407.56118	0.00044	91	−0.00465	(2)	2457701.94521	0.00030	15165	−0.04332	(6)
2454407.66863	0.00058	91.5	−0.00648	(2)	2458033.94637	0.00171	16684	−0.01961	(5)
2454407.66978	0.00500	91.5	−0.00532	(1)	2458034.05805	0.00044	16684.5	−0.01721	(5)
2454407.78173	0.00076	92	−0.00265	(2)	2458034.16574	0.00065	16685	−0.01879	(5)
2454407.78205	0.00085	92	−0.00233	(2)	2458063.77583	0.00050	16820.5	−0.02222	(6)
2454409.63478	0.00200	100.5	−0.00727	(1)	2458063.88463	0.00050	16821	−0.02270	(6)
2454410.62278	0.00600	105	−0.00275	(1)	2458817.36896	0.00004	20268.5	0.01050	(7)
2454419.68562	0.00085	146.5	−0.00974	(2)	2458817.47767	0.00005	20269	0.00994	(7)
2454419.79298	0.00184	147	−0.01165	(2)	2458819.66324	0.00030	20279	0.01001	(6)
2454420.56078	0.00200	150.5	−0.00877	(1)	2458819.77304	0.00090	20279.5	0.01054	(6)
2454436.50978	0.00300	223.5	−0.01392	(1)	2458819.88114	0.00040	20280	0.00936	(6)
2454436.61978	0.00200	224	−0.01320	(1)	2458819.99114	0.00040	20280.5	0.01009	(6)
2454436.72908	0.00080	224.5	−0.01317	(1)	2458823.04993	0.00005	20294.5	0.00917	(7)
2454438.47740	0.00061	232.5	−0.01326	(2)	2458823.15856	0.00007	20295	0.00853	(7)
2454438.47768	0.00070	232.5	−0.01297	(1)	2458830.47879	0.00014	20328.5	0.00733	(7)
2454438.47778	0.00200	232.5	−0.01287	(1)	2458830.58762	0.00008	20329	0.00689	(7)
2454438.58561	0.00053	233	−0.01432	(2)	2458837.03379	0.00007	20358.5	0.00583	(7)
2454438.58678	0.00200	233	−0.01315	(1)	2458837.14253	0.00008	20359	0.00530	(7)
2454438.69678	0.00500	233.5	−0.01242	(1)	2459549.33302	0.00026	23617.5	0.05061	(8)
2454438.69812	0.00144	233.5	−0.01109	(2)	2459574.34923	0.00060	23732	0.04285	(8)
2454439.56978	0.00300	237.5	−0.01363	(1)	2459574.34969	0.00020	23732	0.04331	(8)
2454444.37660	0.00047	259.5	−0.01491	(2)	2459574.34988	0.00010	23732	0.04350	(8)
2455539.48043	0.00300	5270	0.04415	(3)	2459574.45487	0.00060	23732.5	0.03921	(8)
2455539.48060	0.00300	5270	0.04432	(3)	2459574.45772	0.00010	23732.5	0.04206	(8)
2455539.58995	0.00300	5270.5	0.04440	(3)	2459574.45905	0.00120	23732.5	0.04339	(8)
2455539.59006	0.00300	5270.5	0.04451	(3)	2459916.29791	0.00029	25297	−0.03922	(8)
2455570.28832	0.00300	5411	0.03649	(3)	2459916.29829	0.00010	25297	−0.03884	(8)
2455570.28843	0.00300	5411	0.03660	(3)	2459916.29849	0.00011	25297	−0.03864	(8)
2455570.39783	0.00300	5411.5	0.03672	(3)	2459916.40807	0.00016	25297.5	−0.03834	(8)
2455570.39785	0.00300	5411.5	0.03674	(3)	2459916.40828	0.00023	25297.5	−0.03813	(8)
2456671.07877	0.00500	10448	−0.00941	(4)	2459916.40830	0.00021	25297.5	−0.03811	(8)

Reference: (1) Christian et al. (2006), (2) SuperWASP, (3) Dimitrov et al. (2015), (4) Zhang et al. (2014b), (5) ASAS-SN, (6) Lu et al. (2020), (7) TESS, (8) This paper.

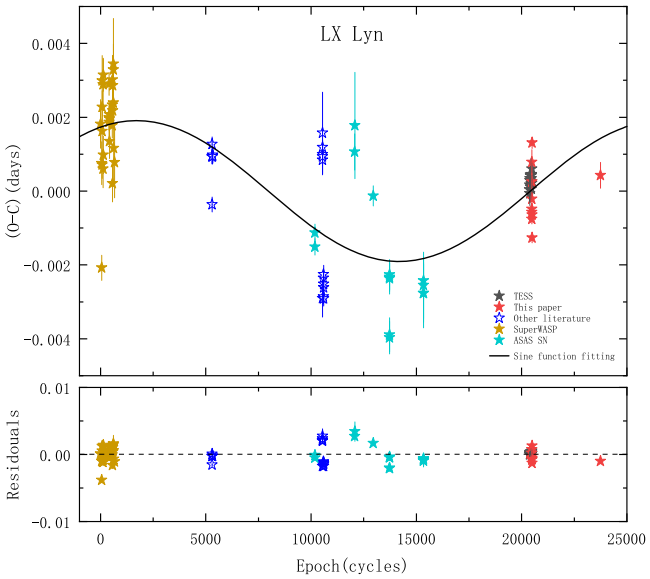

Figure 3. The $O-C$ diagram of LX Lyn formed by all available measurements with the linear ephemeris Equation (1). The black line refers to periodic variation. The corresponding $O-C$ residuals are displayed in the bottom panel.

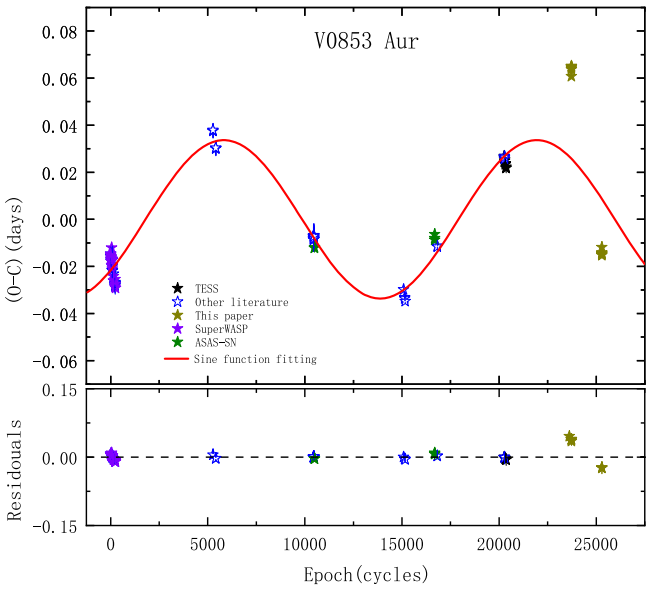

Figure 4. In the top panel, the red line represents, relative to Equation (3), the expected $O-C$ curve based on Equation (4). The $O-C$ residuals are displayed in the bottom panel.

albedo $A_1 = A_2 = 0.5$ (Ruciński 1969), and the gravity-darkening exponents were chosen as $g_1 = g_2 = 0.32$ (Lucy 1967). The bolometric limb-darkening coefficients and limb-darkening coefficients were computed via the linear darkening law from Van Hamme (1993).

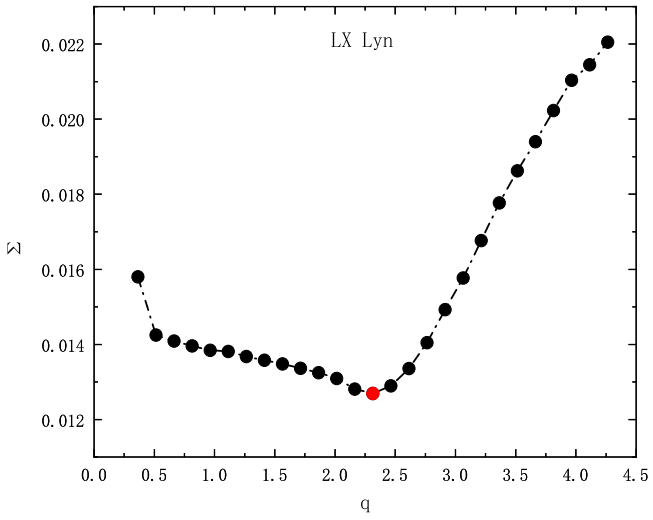

Figure 5. The Σ–q curve determined by the W-D program applied to LX Lyn.

4.1. LX Lyn

Based on the LAMOST data, we set the temperature of the primary to 4780 K (Green et al. 2019). LX Lyn has been classified as a W UMa type EB (Terrell et al. 2014), so we used mode 3 (contact mode) to analyze its LCs. The q-search method is utilized to ascertain the appropriate mass ratio. It is found that the lowest point of the q-search curve is about 2.31. It should be noted that the LCs of LX Lyn have a negative O'Connell effect (O'Connell 1951). In order to fit the LCs of the system better, we adopted a cool starspot model. After many times fitting, we get the best photometric solutions with one spot on the primary component. Our best photometric elements together with the published results are listed in Table 4. The q-search curve of LX Lyn is plotted in Figure 5. The theoretical LCs calculated with the cool-spots are shown in Figure 6 and the geometrical structure of the system is illustrated in Figure 7.

Additionally, we analyzed the LCs from TESS($LC_{\rm TESS2019}$ and $LC_{\rm TESS2021}$), which also exhibit an obvious asymmetry. During our fitting, we also fixed the temperature T_1 at 4780 K and added a cool starspot. It should be noted that $LC_{\rm TESS2019}$ and $LC_{\rm TESS2021}$ show different O'Connell effects. The final photometric solutions are listed in Table 4, and the theoretical LCs are shown in Figure 6(a) and (b), respectively.

4.2. V0853 Aur

Based on published results, the temperature of the primary star was adopted as 5560 K. Using the same method, we fitted the LCs of V0853 Aur with mode 3 and the same adjustable parameters. We noted that the LCs of V0853 Aur still have an obvious asymmetry, and the differential magnitude of phase 0.25 is approximately 0.1 mag less than phase 0.75. So, we

Table 4
Photometric Solutions for LX Lyn

Parameter	Observed Data in 2020		TESS Data		Darwish et al. (2017)	Loukaidou et al. (2022)
	Without Spot	With Spot	2019	2021		
$g_1 = g_2$	0.32	0.32	0.32	0.32	0.32	
$A_1 = A_2$	0.50	0.50	0.50	0.50	0.50	
T_1^a(K)	4780	4780	4780	4780	4589	4650
$q = \frac{M_2}{M_1}$	2.3139 (±0.0285)	2.3139[a]	2.3870 (±0.0251)	2.3950 (±0.0040)	0.4732 (±0.0018)	0.451 (±0.0012)
T_2(K)	4708 (±0.0008)	4696 (±0.0010)	4704 (±0.0006)	4686 (±0.0002)	4581 (±3)	4720(± 12)
$i(^\circ)$	84.882 (±0.5522)	85.245 (±0.6294)	85.546 (±0.5336)	83.979 (±0.0641)	82.70 (±0.27)	86.3 (±1.2)
$\frac{L_1}{L_1+L_2}$(TESS)			0.3427 (±0.0202)	0.3428 (±0.0091)		
$\frac{L_1}{L_1+L_2}(V)$	0.3408 (±0.0330)	0.3450 (±0.0346)				
$\frac{L_1}{L_1+L_2}(R_c)$	0.3358 (±0.0464)	0.3391 (±0.0434)				
$\frac{L_1}{L_1+L_2}(I_c)$	0.3329 (±0.0664)	0.3357 (±0.0559)				
$\Omega_1 = \Omega_2$	5.6222 (±0.0357)	5.6140 (±0.0089)	5.5917 (±0.0330)	5.7266 (±0.0037)	2.7641 (±0.0046)	2.755 (±0.023)
r_1(pole)	0.2937 (±0.0009)	0.2945 (±0.0007)	0.3022 (±0.0009)	0.2917 (±0.0002)	0.4293 (±0.0027)	
r_1(side)	0.3071 (±0.0010)	0.3080 (±0.0009)	0.3177 (±0.0010)	0.3050 (±0.0002)	0.4590 (±0.0036)	0.4557
r_1(back)	0.3436 (±0.0013)	0.3449 (±0.0014)	0.3635 (±0.0014)	0.3418 (±0.0004)	0.4910 (±0.0520)	
r_2(pole)	0.4329 (±0.0037)	0.4323 (±0.0007)	0.4452 (±0.0034)	0.4350 (±0.0004)	0.3064 (±0.0039)	
r_2(side)	0.4627 (±0.0050)	0.4619 (±0.0009)	0.4788 (±0.0047)	0.4652 (±0.0005)	0.3213 (±0.0048)	0.3097
r_2(back)	0.4923 (±0.0070)	0.4914 (±0.0012)	0.5125 (±0.0068)	0.4944 (±0.0007)	0.3617 (±0.0088)	
Spot		Primary	Primary	Primary		
Latitude(°)		29.0029 (±0.2731)	16.1479 (±0.0375)	33.8607 (±0.0101)		
Longitude(°)		253.0860 (±0.1326)	296.8894 (±0.2284)	272.9014 (±0.0287)		
Radius(°)		24.9032 (±0.1305)	24.9032[a]	24.9032[a]		
T_s^a		0.8054	0.8054	0.8054		
Mean residual	0.01	0.01	0.0024	0.002	0.0073	

Reference: Fixed parameters in our analysis.

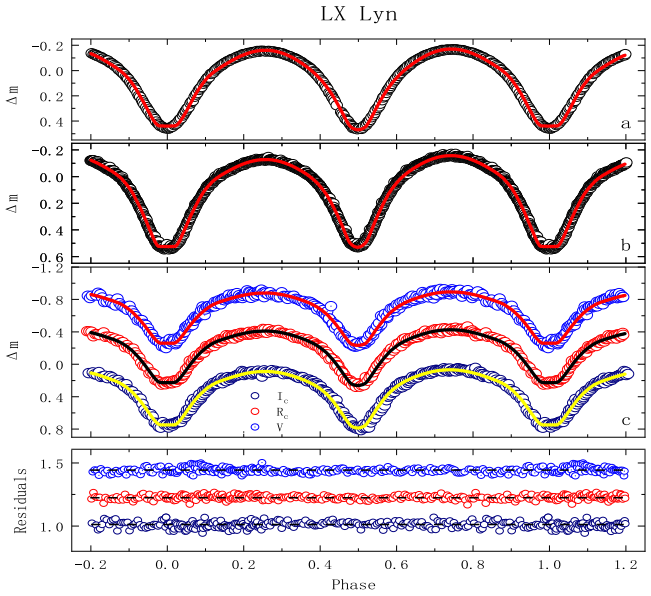

Figure 6. The different colored circles represent observed data, and the solid lines are theoretical LCs with cool starspots. The fitting residuals in different bands are plotted in the bottom panel. The LCs from TESS are depicted in Figure 6(a)(TESS2019) and Figure 6(b)(TESS2021)

added the cool starspot during our analysis. At the beginning, we carried out a q-search ranging from 0.1 to 5 for the mass ratio. The q-search result shows that the possible value of the mass ratio is near $q = 2.7727$. Subsequently, we input the value of mass ratio as $q = 2.7727$, and set it as an adjustable parameter. In order to get the best photometric results, a third light (l_3) is also added. The final photometric solutions are listed in Table 5. The q-search curve of V0853 Aur is plotted in Figure 8. The theoretical LCs of TESS and ours are shown in Figure 9(a) and (b), respectively. The geometric structure of the system is illustrated in Figure 10.

5. Discussion and Conclusion

In Section 3, we analyzed the orbital period variations of LX Lyn and V0853 Aur. In Section 4, after fitting LCs of the targets, we obtained their photometric solutions. In this section, we will discuss the results of the above two sections in detail.

5.1. Photometric Solution

Based on the photometric results, we calculate the contact degree as $f = 12\%$, indicating that LX Lyn is a shallow-contact

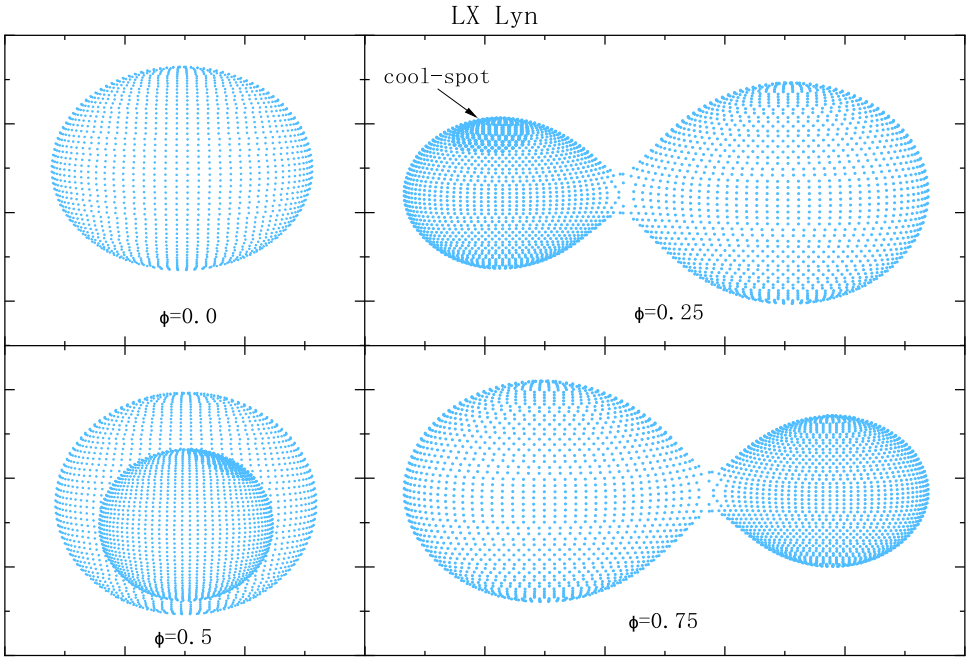

Figure 7. Geometric structure of LX Lyn at phases of 0, 0.25, 0.5, and 0.75.

EB. We found that LX Lyn is a W-subtype EB with a mass ratio of $q = 2.31$ and an orbital inclination of $i = 84.^{\circ}88$. The temperature difference between the two components is about $\Delta T = 72$ K. At the same time, the photometric solutions of TESS LCs from sector 20 and 47 are similar, although they have different exposure times. In addition, we also calculated the fundamental parameters of the target by using the empirical formula provided by Gazeas (2009),

$$\log M_1 = 0.725(59) \cdot \log P - 0.076(32) \cdot \log q + 0.365(32) \quad (5)$$

$$\log M_2 = 0.725(59) \cdot \log P + 0.924(33) \cdot \log q + 0.365(32) \quad (6)$$

$$\log R_1 = 0.930(27) \cdot \log P - 0.141(14) \cdot \log q + 0.434(14), \quad (7)$$

$$\log R_2 = 0.930(29) \cdot \log P + 0.287(15) \cdot \log q + 0.434(16), \quad (8)$$

$$\log L_1 = 2.531(67) \cdot \log P - 0.512(51) \cdot \log q + 1.102(43), \quad (9)$$

$$\log L_2 = 2.531(63) \cdot \log P + 0.352(52) \cdot \log q + 1.102(41), \quad (10)$$

where p is orbital period, q is mass ratio, M is the mass, R is the radius and L is the luminosity. The fundamental parameters we calculated for LX Lyn are $M_1 = 0.311M_{\odot}$, $M_2 = 0.719M_{\odot}$, $R_1 = 0.584R_{\odot}$, $R_2 = 0.836R_{\odot}$, $L_1 = 0.173L_{\odot}$ and $L_2 = 0.358L_{\odot}$ (Table 6), respectively. The LCs of LX Lyn show a negative O'Connell effect, which could be caused by magnetic activity from the components. In Table 4, we noted that the parameters of cool starspots are somewhat different, which could be the result of the evolution of the starspots themselves (Zhang et al. 2014a). We also noted that the mass ratio of Loukaidou et al. (2022) is $q = 0.451$, which is exactly the reciprocal of $q = 2.31$. The photometric solutions reveal that LX Lyn is a totally EB system with a high orbital inclination (>85°), so our photometric physical parameters are reliable (Li et al. 2022).

Using the same method, we also obtained the photometric solutions of V0853 Aur. It is suggested that V0853 Aur is a W-subtype CEB with a mass ratio of $q = 2.77$. The contact degree ($f = 26.3\%$) reveals that it is a medium contact system with a similar surface temperature of the components ($\Delta T = 276$ K). According to Kepler's third law, we calculated the semimajor axis of the orbit to be $a = 1.510R_{\odot}$. Based on the photometric results, using the empirical formula provided by Gazeas (2009), the mass, radius and luminosity of the target were calculated as $M_1 = 0.257M_{\odot}$, $M_2 = 0.712M_{\odot}$, $R_1 = 0.572R_{\odot}$, $R_2 = 0.885R_{\odot}$, $L_1 = 0.160L_{\odot}$ and $L_2 = 0.386L_{\odot}$, respectively. Due to the LCs of the system being asymmetric, we adopted a cool starspot model. A cool starspot on the surface of a star can destroy the symmetry of the LCs (Zhou et al. 2016; Zhang et al. 2018a). It should be noted that our photometric solutions have a significant difference with previously published results, such as the orbital inclination (i) and effective temperature of the secondary component (T_2). One main reason for that is the migration of cool starspots. With the evolution of cool starspots, the photometric solutions of the target will be affected, such as V410 Aur (Liao et al. 2022) and EE Cet (Yang & Wang 2023). Moreover, we also found the third light

Table 5
Photometric Solutions for V0853 Aur

Parameter	Observed Data in 2021		TESS Data	Zhang et al. (2014b)	Lu et al. (2020)
	Without Spot	With Spot			
$g_1 = g_2^a$	0.32	0.32	0.32		
$A_1 = A_2^a$	0.50	0.50	0.50		
T_1(K)^a	5560	5560	5560	4839 (±4)	6664
$q = \frac{M_2}{M_1}$	2.7727 (±0.0360)	2.7727^a	2.7727 (±0.0256)	2.74 (±0.01)	0.300 (±0.001)
T_2(K)	5284 (±0.0021)	5275 (±0.0019)	5286 (±0.0007)	4750^a	6817 (±21)
i(°)	79.259 (±1.3452)	80.103 (±0.7705)	80.197 (±0.5186)	72.13 (±0.06)	73.53 (±0.03)
$\frac{L_1}{L_1+L_2}$(TESS)			0.3515 (±0.0091)		
$\frac{L_1}{L_1+L_2}(B)$				0.313 (±0.001)	0.72 (±0.02)
$\frac{L_1}{L_1+L_2}(V)$	0.3385 (±0.0285)	0.3402 (±0.0164)		0.307 (±0.001)	0.73 (±0.02)
$\frac{L_1}{L_1+L_2}(R_c)$	0.3305 (±0.0233)	0.3320 (±0.0143)			0.73 (±0.02)
$\frac{L_1}{L_1+L_2}(I_c)$	0.3235 (±0.0218)	0.3247 (±0.0146)			0.74 (±0.02)
$\frac{L_3}{L_1+L_2+L_3}$(TESS)			0.2315 (±0.0032)		
$\frac{L_3}{L_1+L_2+L_3}(V)$	0.1879 (±0.0072)	0.1812 (±0.0045)			
$\frac{L_3}{L_1+L_2+L_3}(R_c)$	0.2308 (±0.0057)	0.2296 (±0.0037)			
$\frac{L_3}{L_1+L_2+L_3}(I_c)$	0.2900 (±0.0052)	0.2904 (±0.0035)			
$\Omega_1 = \Omega_2$	6.1520 (±0.0327)	6.1562 (±0.0423)	5.9255 (±0.0060)	6.211 (±0.003)	2.424 (±0.001)
r_1(pole)	0.2866 (±0.0013)	0.2870 (±0.0012)	0.3053 (±0.0005)		0.5 (±0.2)
r_1(side)	0.3003 (±0.0016)	0.3008 (±0.0014)	0.3235 (±0.0007)		0.5 (±0.3)
r_1(back)	0.3422 (±0.0033)	0.3433 (±0.0024)	0.3900 (±0.0016)		0.5 (±0.4)
r_2(pole)	0.4506 (±0.0031)	0.4514 (±0.0039)	0.4694 (±0.0005)		0.3 (±0.2)
r_2(side)	0.4846 (±0.0044)	0.4856 (±0.0054)	0.5107 (±0.0007)		0.3 (±0.3)
r_2(back)	0.5146 (±0.0061)	0.5157 (±0.0075)	0.5493 (±0.0009)		0.3 (±0.5)
Spot		Primary	Primary	Primary	Primary
Latitude(°)		153.0562 (±0.0291)	153.7845 (±0.0105)	146.2 (±2.3)	90^a
Longitude(°)		273.2034 (±0.1109)	237.0269 (±0.0407)	278.6 (±0.9)	241.4 (±0.4)
Radius(°)		41.3965^a	41.3966^a	54.2 (±0.3)	22.7 (±0.3)
T_s^a		0.7595	0.7595	0.970 (±0.002)	0.9258 (±0.0061)
Mean residual	0.0016	0.0011	0.0018		0.24

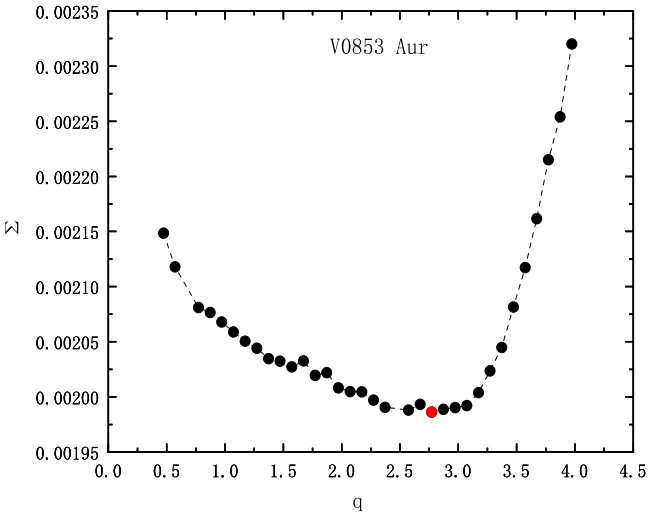

Figure 8. The q-search curve of V0853 Aur.

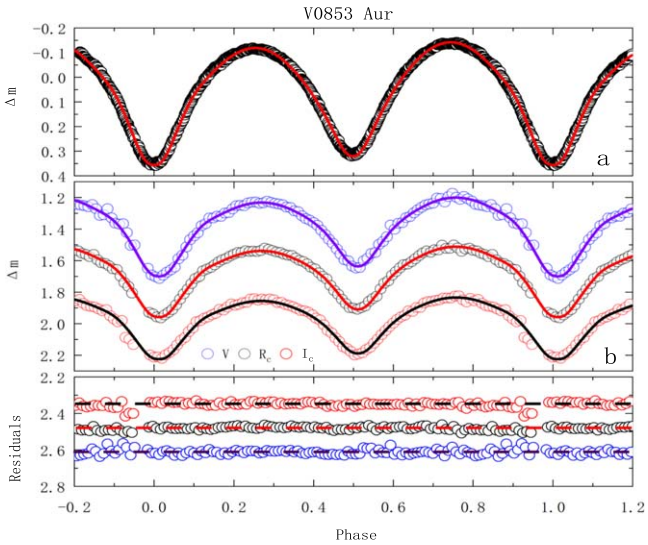

Figure 9. Observational LCs of V0853 Aur along with the theoretical fits.

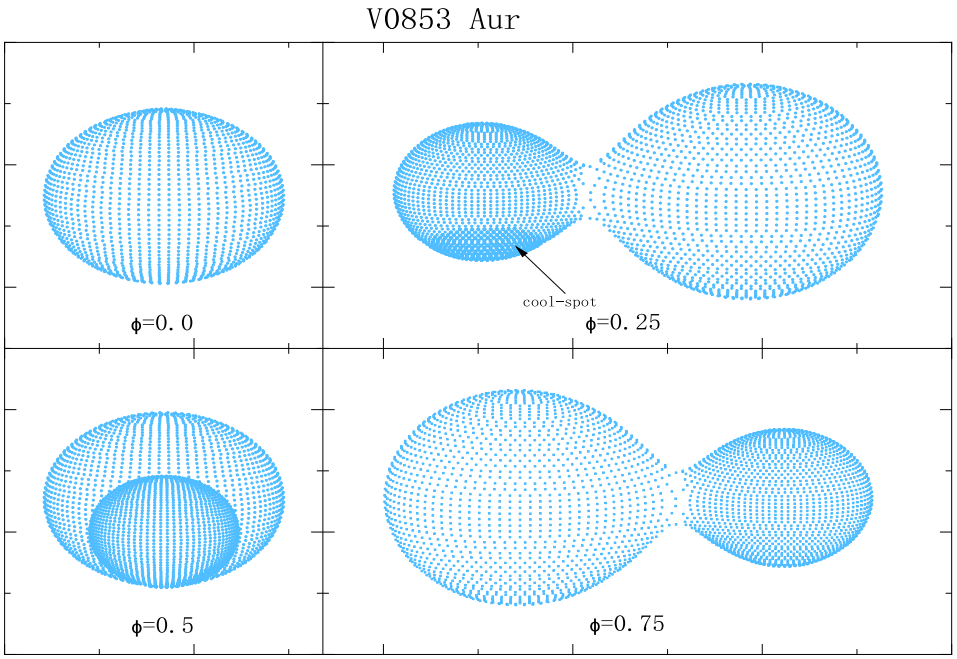

Figure 10. Geometric configuration of V0853 Aur at the phases of 0, 0.25, 0.5 and 0.75.

Table 6
The Fundamental Parameters for LX Lyn and V0853 Aur

Parameter	$M_1(M_\odot)$	$M_2(M_\odot)$	$R_1(R_\odot)$	$R_2(R_\odot)$	$L_1(L_\odot)$	$L_2(L_\odot)$	$a(R_\odot)$
LX Lyn	0.311	0.719	0.584	0.836	0.173	0.358	1.537
	±0.045	±0.095	±0.073	±0.019	±0.022	±0.042	±0.025
V0853 Aur	0.257	0.712	0.572	0.885	0.160	0.386	1.510
	±0.034	±0.094	±0.074	±0.015	±0.024	±0.058	±0.027

Table 7
Parameters of the Third Body for LX Lyn

Parameter	Value	Error	Unit
P_3	14.8363	±0.55	yr
A	0.00191	±0.0007	day
$a_{12}\sin i$	0.33095	±0.0123	au
f(m)	0.000165	±0.0001	$M_\odot$
$M_3(i = 90°)$	0.06	±0.02	$M_\odot$

Table 8
Parameters of the Third Body for V0853 Aur

Parameter	Value	Error	Unit
P_3	9.6446	±0.0166	yr
A	0.0337	±0.0006	day
$a_{12}\sin i$	5.8308	±0.015	au
f(m)	2.1335	±0.0785	$M_\odot$
$M_3(i = 90°)$	3.77	±0.06	$M_\odot$

during our analysis, and the existence of the third light is another important reason. It should be noted that the parameters of the starspot are somewhat different, which could be the result of the evolution of starspots (Zhang et al. 2014b; Zhang et al. 2019).

5.2. Orbital Period Variation

By using the $O-C$ method, we found that the $O-C$ curves of LX Lyn and V0853 Aur show periodic variations. At present, cyclic period changes can be explained as resulting either from the magnetic activity of one or both components (Applegate 1992). If magnetic activity is the main reason, variations in the gravitational quadrupole moment (ΔQ) may result in observed oscillations (Zhang et al. 2018b). The changes of gravitational quadrupole moment $\triangle Q$ can be calculated according to the following two formulas (Lanza & Rodonò 2002),

$$\triangle P = A\sqrt{2[1 - \cos(2\pi P/P_3)]}, \quad (11)$$

Table 9
Some CEB Systems with a Third Body

Name	P (days)	P_3 (yr)	q (M_2/M_1)	M_1 ($M_\odot$)	M_2 ($M_\odot$)	R_1 ($R_\odot$)	R_2 ($R_\odot$)	T_1 (K)	$M_{3\,\mathrm{min}}$ ($M_\odot$)	f Filling-out Factor	Reference
V0853 Aur	0.21855	9.64	2.77	0.26	0.71	0.57	0.89	5560	3.77	26.3%	(1)
		±0.017	±0.036	±0.034	±0.094	±0.074	±0.015		±0.063	±0.5%	
LX Lyn	0.21751	14.84	2.31	0.31	0.72	0.59	0.84	4780	0.06	12%	(1)
		±0.552	±0.029	±0.045	±0.095	±0.073	±0.019		±0.013	±1%	
HH UMa	0.37549	19.25	0.30	1.22	0.36	1.34	0.83	6550	0.26	66%	(2)(3)
		±0.520		±0.020	±0.010	±0.010	±0.010		±0.153	±2%	
V471 Cas	0.33600	12.80	0.64	0.65	0.41	0.99	0.81	5975	0.12	8%	(4)
		±0.110	±0.043	±0.041	±0.041	±0.031	±0.031				
KIC 9532219	0.19815	3.27	1.20	0.72	0.86	0.60	0.66	5203	0.09		(5)
		±0.295	±0.212	±0.233	±0.244	±0.266	±0.231		±0.331		
V0644 Ser	0.22072	9.15	1.95	0.29	0.56	0.48	0.65	4750	0.11	14%	(6)
		±5.05	±0.139	±0.411	±0.450	±0.414	±0.520		±0.167	±0.5%	
V1110 Per	0.22815	15.86	0.65	0.84	0.55	0.74	0.67	5350	0.53	29%	(7)
		±5.05	±0.022	±0.010	±0.022	±0.009	±0.009		±0.14	±7%	
V0441 UMa	0.22771	14.50	0.40	0.85	0.34	0.80	0.50	4700	0.08	19%	(7)
		±0.01		±0.005	±0.006	±0.054	±0.034		±0.01	±2%	
AE Crv	0.22637	14.90	0.40	0.85	0.34	0.79	0.54	4650	0.11	10%	(7)
		±1.74	±0.283	±0.001	±0.024	±0.044	±0.030		±0.02	±9%	
NSVS 13392702	0.26006	3.86	0.51	0.93	0.48	0.87	0.61	5150	0.10	11%	(7)
		±0.04		±0.007	±0.030	±0.052	±0.036		±0.01	±9%	
V1498 Her	0.22371	9.55	0.66	0.83	0.54	0.75	0.59	4700	0.27	13%	(7)
		±0.01	±0.033	±0.010	±0.028	±0.013	±0.010		±0.01	±7%	
V1067 Her	0.25811	49.02	0.58	0.92	0.54	0.86	0.64	5300	0.22	13%	(7)
		±3.20	±0.036	±0.010	±0.034	±0.017	±0.013		±0.01	±7%	
2MASS J21042404 +0731381	0.20909	2.78	0.31	0.81	0.25	0.75	0.41	4800	0.28	3%	(7)
		±0.05	±0.041	±0.005	±0.033	±0.023	±0.013		±0.01	±2%	
1SWASP J212454.61 +203030.8	0.22783	8.78	0.43	0.85	0.36	0.78	0.50	5250	0.28	5%	(7)
		±0.94	±0.007	±0.002	±0.006	±0.004	±0.004		±0.01	±5%	
V0694 Peg	0.22484	13.57	0.37	0.84	0.40	0.78	0.53	4700	0.06	16%	(7)
		±1.52	±0.047	±0.004	±0.040	±0.023	±0.016		±0.01	±8%	

Reference: (1) This paper, (2) Wang et al. (2015), (3) Chang et al. (2023), (4) Kjurkchieva et al. (2019), (5) Lee et al. (2016), (6) Xu et al. (2022), (7) Loukaidou et al. (2022).

$$\frac{\triangle P}{P} = -9\frac{\triangle Q}{M_{1,2}a^2}, \tag{12}$$

where a is the separation between both components and M is the mass of the active component (Yang et al. 2012). For LX Lyn, we can compute the values of ΔQ as follows, $\Delta Q_1 = 2.47 \times 10^{48}\,\mathrm{g\,cm^2}$ and $\Delta Q_2 = 5.70 \times 10^{48}\,\mathrm{g\,cm^2}$. For V0853 Aur, we get the values of $\Delta Q_1 = 5.33 \times 10^{49}\,\mathrm{g\,cm^2}$ and $\Delta Q_2 = 1.48 \times 10^{50}\,\mathrm{g\,cm^2}$. These results are evidently smaller than the typical values of 10^{51}–$10^{52}\,\mathrm{g\,cm^2}$ for close binaries (Lanza & Rodonò 1999; Yang et al. 2014). Therefore, we can rule out the Applegate mechanism as a main reason for interpreting the cyclic variations of LX Lyn and V0853 Aur at present.

In the situation of LTTE working in a circular orbit, we calculated the parameters of the third body and listed them in Tables 7 and 8. According to the results of our analysis, the orbital period of the tertiary component of LX Lyn is $P_3 = 14.84$ yr, and the amplitude is $A = 0.00191$ days. For V0853 Aur, its period is $P_3 = 9.64$ yr and the amplitude is $A = 0.0337$ days. According to the $O-C$ fitting parameters, the distance of the binary system to the barycenter of the triple system can be calculated with the equation,

$$a_{12}\sin i_3 = A_3 \times c, \tag{13}$$

where c is the speed of the light and A_3 is the amplitude of the $O-C$ oscillation, i.e., $a_{12}\sin i = 0.331$ au (LX Lyn) and $a_{12}\sin i = 5.83$ au (V0853 Aur). The mass function and the mass of the tertiary companion are computed with

$$f(m) = \frac{4\pi^2}{GP_3^2} \times (a_{12}\sin i)^3 = \frac{(M_3\sin i)^3}{(M_1+M_2+M_3)^2}, \tag{14}$$

and we could get the minimum mass of the third body with the orbital inclination of $i_3 = 90°$. The $M_{3\,\mathrm{min}}$ of LX Lyn is $0.06M_\odot$. For LX Lyn, it should be noted that we did not find the third

light during our analysis, so we guess that the tertiary companion might be a low mass M-type star or brown dwarf. For V0853 Aur, the $M_{3\,\mathrm{min}}$ we calculated is about $3.77M_{\odot}$. A third light was found during our fitting, so we think that the third body of V0853 Aur could be a massive star.

Usually, for low mass EBs, the timescale of the AML is very long, and it is difficult to become a CEB with a period shorter than 0.22 days (Zhou et al. 2016; Zhang et al. 2019). As discussed by Qian et al. (2015), the magnetic torques from stellar winds could speed up the AML, which is good for the formation of a CEB. Meanwhile, Lu et al. (2020) and Dimitrov & Kjurkchieva (2015) reported that the components of two targets show strong magnetic activities, e.g., the chromospheric emission lines and the stellar spots on the photospheres. We also thought that the third body might extract angular momentum from the central binary system during the early dynamical interaction or late evolution, which could also shorten the time of orbital evolution for these EBs (Liao & Qian 2010; Zhou et al. 2016; Li et al. 2021). So, the orbital shrinkage due to rapid AML may result in the formation of contact systems similar to LX Lyn and V853 Aur.

In addition, we also collect the fundamental parameters of some short-period contact binaries with a third body, and list them in Table 9. From Table 9, it is discovered that many of the components of these systems are late-type stars with a mass less than $1M_{\odot}$. Most of these systems are shallow CEBs, and their third bodies are usually low-mass stars, except for V0853 Aur. Another special case is WW Dra, and a study suggested that the mass of its third body is no less than $6.43M_{\odot}$ (Liao & Qian 2010). More observations (photometric and spectroscopic) are still necessary to verify results in the future.

Acknowledgments

This work is partly supported by the Joint Research Fund in Astronomy (grant Nos. U1931101, 42364001) under cooperative agreement between the National Natural Science Foundation of China (NSFC) and Chinese Academy of Sciences (CAS), the National Natural Science Foundation of China (NSFC, Grant No. 11933008), the Guizhou Provincial Science and Technology Foundation (grant Nos. [2020]1Y017, ZK[2022]322), and the Foundation of Education Bureau of Guizhou Province, China (grant No. KY (2020) 003). We acknowledge the support of the staff of the Xinglong 60 and 80 cm telescopes. This work was partially supported by the Open Project Program of the CAS Key Laboratory of Optical Astronomy, National Astronomical Observatories, Chinese Academy of Sciences. This work includes data collected by the TESS mission, and we acknowledge the TESS team for its support.

References

Applegate, J. H. 1992, ApJ, 385, 621
Binnendijk, L. 1970, VA, 12, 217
Borkovits, T., Hajdu, T., Sztakovics, J., et al. 2016, MNRAS, 455, 4136
Chang, L.-F., Zhu, L. -Y., & Meng, F.-B. 2023, RAA, 23, 045017
Christian, D. J., Pollacco, D. L., Skillen, I., et al. 2006, MNRAS, 372, 1117
Darwish, M. S., Elkhateeb, M. M., Nouh, M. I., et al. 2017, NewA, 50, 37
Davenport, J. R. A., Becker, A. C., West, A. A., et al. 2013, ApJ, 764, 62
Dimitrov, D. P., & Kjurkchieva, D. P. 2015, MNRAS, 448, 2890
Drake, A. J., Djorgovski, S. G., Garcalvarez, D., et al. 2014, ApJ, 790, 157
Eker, Z., Soydugan, F., Soydugan, E., et al. 2015, AJ, 149, 131
Gazeas, K. D. 2009, CoAst, 159, 129
Green, G. M., Schlafly, E. Z. C., Speagle, J. S., et al. 2019, ApJ, 887, 93
Hoffman, D. I., Harrison, T. E., & McNamara, B. J. 2009, AJ, 138, 466
Irwin, John B. 1952, ApJ, 116, 211
Jiang, D. K., Han, Z. W., Ge, H. W., et al. 2012, MNRAS, 421, 2769
Kjurkchieva, D. P., Popov, V. A., Eneva, Y., et al. 2019, RAA, 19, 14
Lanza, A. F., & Rodonò, M. 1999, A&A, 349, 887
Lanza, A. F., & Rodonò, M. 2002, AN, 323, 424
Lee, J. W., Hong, K., & Koo, J. R. 2016, ApJ, 820, 1
Li, K., Gao, X., Liu, X. Y., et al. 2022, AJ, 164, 202
Li, K., Xia, Q. Q., Kim, C.-H., et al. 2021, AJ, 162, 13
Li, L. F., Han, Z. W., & Zhang, F. H. 2004, MNRAS, 355, 1383
Li, L. F., Zhang, F. H., Han, Z. W., & Jiang, D. K. 2007, ApJ, 662, 596
Liao, W. P., & Qian, S. B. 2010, yCat, 1, 74051930L
Liao, W. P., Qian, S. B., Shi, X.-D., et al. 2022, ApJ, 927, 183
Lohr, M. E., Norton, A. J., Kolb, U. C., et al. 2013, A&A, 549, 86
Loukaidou, G. A., Gazeas, K. D., Palafouta, S., et al. 2022, MNRAS, 514, 5528
Lu, H. P., Zhang, L. Y., Michel, R., et al. 2020, ApJ, 901, 169
Lucy, L. B. 1967, ZA, 65, 89
Lucy, L. B. 1968, ApJ, 151, 1123
Lucy, L. B. 1973, Ap&SS, 22, 381
Nefs, S. V., Birkby, J. L., Snellen, I. A. G., et al. 2012, MNRAS, 425, 950
Norton, A. J., Payne, S. G., Evans, T., et al. 2011, A&A, 528, 90
O'Connell, D. J. K. 1951, MNRAS, 111, 642
Pribulla, T., & Rucinski, S. M. 2006, AJ, 131, 2986
Qian, S.-B. 2003, MNRAS, 342, 1260
Qian, S. B., He, J. J., Zhang, J., et al. 2017, RAA, 17, 87
Qian, S.-B., Liu, N.-P., Li, K., et al. 2013, ApJS, 209, 13
Qian, S. B., Zhang, J., He, J. J., et al. 2018, ApJS, 235, 5
Qian, S.-B., Zhou, X., Zhu, L.-Y., et al. 2015, AJ, 150, 193
Ruciński, S. M. 1969, AcA, 19, 245
Rucinski, S. M. 1992, AJ, 103, 960
Stępień, K. 2006, AcA, 56, 347
Stępień, K., & Gazeas, K. 2012, AcA, 62, 153
Terrell, D., & Gross, J. 2014, IBVS, 6104, 1T
Van Hamme, W. 1993, AJ, 106, 2096V
Van Hamme, W., & Wilson, R. E. 2003, ASPC, 298, 323
Van Hamme, W., & Wilson, R. E. 2007, ApJ, 661, 1129
Vant Veer, F. 1979, A&A, 80, 287
Wang, K., Zhang, X., & Deng, L. 2015, ApJ, 805, 22
Wilson, R. E. 1979, ApJ, 234, 1054
Wilson, R. E. 1990, ApJ, 356, 613
Wilson, R. E. 1993, ASPC, 38, 91
Wilson, R. E. 2008, ApJ, 672, 575
Wilson, R. E. 2012, AJ, 144, 73
Wilson, R. E., & Devinney, E. J. 1971, ApJ, 166, 605
Wilson, R. E., & Van Hamme, W. 2014, ApJ, 780, 151
Wilson, R. E., Van Hamme, W., & Terrell, D. 2010, ApJ, 723, 1469
Xu, H. S., Zhu, L. Y., et al. 2022, RAA, 22, 5024
Yang, Y.-G., & Wang, S. 2023, NewA, 98, 101919
Yang, Y.-G., Yang, Y., & Li, S.-Z. 2014, AJ, 147, 145
Yang, Y.-G., Zhang, X.-B., Li, H.-L., et al. 2012, AJ, 144, 136
Zhang, B., Qian, S.-B., Liao, W.-P., et al. 2018a, RAA, 18, 116
Zhang, B., Qian, S.-B., Michel, R., et al. 2018b, RAA, 18, 30
Zhang, B., Qian, S.-B., Wang, J.-J., et al. 2020, RAA, 20, 47
Zhang, B., Qian, S.-B., Zhi, Q.-J., et al. 2019, PASP, 131, 034201
Zhang, L.-Y., Pi, Q.-F., & Yang, Y.-G. 2014a, MNRAS, 442, 2620
Zhang, X. B., Deng, L. C., Wang, K., et al. 2014b, AJ, 148, 40
Zhang, X.-D., & Qian, S. B. 2020, MNRAS, 497, 3493
Zhou, X., Qian, S.-B., Zhang, J., et al. 2016, ApJ, 817, 133
Zhou, X., & Soonthornthum, B. 2019, PASJ, 71, 39
Zhou, X., Soonthornthum, B., Qian, S.-B., et al. 2019, MNRAS, 489, 4760